Mem. S.A.It. Vol. 93, 64
© SAIt 2022
Memorie della

Quasars at High-Redshift: Physics and Cosmology

G. Risaliti[1,2], A. Caccianiga[3], R. Gilli[4], M. Paolillo[5,6,7], L. Amati[4], G. Bargiacchi[8,6], S. Belladitta[3,9], D. Dallacasa[10,11], A. Diana[3,12], T. Di Girolamo[5,6], F. Haardt[9], L. Ighina[3,9], E. Lusso[1,2], S. Marchesi[4], A. Moretti[3], R. Nanni[13], E. Nardini[2], A. Peca[14], E. Piedipalumbo[5,6] A. Sacchi[1], T. Sbarrato[3], P. Severgnini[3], M. Signorini[1,2], C. Spingola[10,11], B. Trefoloni[1,2]

[1] Dipartimento di Fisica e Astronomia, Università degli Studi di Firenze, Via G. Sansone 1, I-50019 Sesto Fiorentino (FI), Italy.e-mail: guido.risaliti@unifi.it
[2] Istituto Nazionale di Astrofisica – Osservatorio Astrofisico di Arcetri, Largo E. Fermi 5, Via Tiepolo 11, I-50125 Firenze, Italy
[3] INAF - Osservatorio Astronomico di Brera, via Brera 28, I-20121 Milan, Italy
[4] INAF – Osservatorio di Astrofisica e Scienza dello Spazio di Bologna, Via P. Gobetti 93/3, 40129 Bologna, Italy
[5] Dipartimento di Fisica, Università degli studi di Napoli Federico II, Via Cinthia, 80126 Napoli, Italy
[6] INFN – Sezione di Napoli, Via Cinthia 9, 80126 Napoli, Italy
[7] INAF – Osservatorio Astronomico di Capodimonte, Via Moiariello 16, 80131 Napoli, Italy
[8] Scuola Superiore Meridionale, Largo S. Marcellino 10, 80138 Napoli, Italy
[9] DiSAT – Università degli Studi dell'Insubria, Via Valleggio 11, 22100 Como, Italy
[10] Dipartimento di Fisica e Astronomia, Università degli Studi di Bologna, Via Gobetti 93/2, 40129 Bologna, Italy
[11] INAF – Istituto di Radioastronomia, Via Gobetti 101, 40129 Bologna, Italy
[12] Dipartimento di Fisica G. Occhialini – Università degli Studi di Milano Bicocca, Piazza della Scienza 3, 20126 Milano
[13] Leiden Observatory, P.O. Box 9513, NL-2300 RA Leiden, The Netherlands
[14] University of Miami, Department of Physics, Coral Gables, FL

Received: 7 February 2022; Accepted: 16 June 2022

Abstract. We report on an observational research program aimed at studying the physical properties, the environment and the cosmological relevance of high-redshift quasars. We have been awarded the largest XMM-Newton AO16 program (1.05 Msec) to study z>3 quasars, and a large (500 ks) Chandra program to investigate the environment of a z=6.31 quasar. Our objectives were: -use quasars as standard candles in the Hubble Diagram of quasars, in order to constrain the cosmological model at high redshift; -investigate quasar variability at all redshifts and luminosities with unprecedented detail; - characterize the multiwavelength emission of z=6 quasars, and their environment; obtain an unbiased and complete census of high-z blazars.

Key words. galaxies:active — quasars:general -– quasars:supermassive black holes -– methods:statistical

1. Introduction

X-ray observations of high-redshift quasars are fundamental to solve some of the most outstanding issues in the fields of AGN-galaxy interaction, galaxy/AGN evolution, and cosmology. In particular: 1) We recently demonstrated that the non-linear correlation between X-ray and UV emission in quasars can be used to estimate quasar distances with a precision of ∼0.2 dex (Lusso & Risaliti 2016). This allows us to build a Hubble Diagram for quasars up to z∼6, opening a new window of observational cosmology at high redshift (Risaliti & Lusso 2015). In particular, this new Hubble diagram allows to tests cosmological scenarios different from the standard flat-ΛCDM model. Considering the equation of state of the dark energy component, $w = p(z)/u(z)$, where $p(z)$ and $u(z)$ are the pressure and energy density, respectively ($w = -1$ in a ΛCDM model), it is possible to investigate cases with a redshift dependence of the parameter w, which are almost perfectly degenerate in the Hubble diagram at low redshifts, but can be separated at $z > 2$. The observed dispersion of the relation is mostly due to X-ray variability and to unaccounted X-ray spectral and calibration issues. For this reason, we need (a) dedicated pointed X-ray observations of very luminous quasars, and (b) an accurate analysis of quasar variability at high redshifts. Regarding the first point, in 2016 we have been awarded an XMM-Newton Very Large Program (the largest approved in AO16) to observe a sample of 30 quasars at z∼3.0-3.3, with SDSS spectra. The main objective was the measurement of the expansion rate of the Universe at z∼3 with a 8% precision, enough for a tight test of the standard cosmological model, and for an improvement of current constraints on the possible evolution of dark energy. For the second point, we need an extensive study of AGN optical and X-ray variability, in order to characterize the temporal properties of high-z AGNs and to derive masses and accretion rates over cosmic times, using archival data and simulations (Paolillo et al. 2017). 2) The formation of supermassive black holes (SMBHs) at galaxy centers is still not well understood. Wide-area optical surveys have already discovered about 300 QSOs at z∼6. The brightest of these QSOs are powered by SMBHs bigger than 10^9 $M_\odot$, even reaching $\sim 10^{10}$ $M_\odot$ (Wu et al. 2015). Understanding how they could form and grow in less than 1 Gyr, i.e. the age of the Universe at z=6, is a challenge for both theory and observations. If they formed through a continuous accretion close to the Eddington limit of small seeds, it is expected to find them in regions with an overdensity of galaxies. Currently, observations lag behind theoretical modeling, and there is still no direct measurement of the environment around early SMBHs. In 2015 we were granted a Chandra Large Program (Cycle 17) to observe for 500ks the field around the z=6.31 QSO SDSS J1030+0524 (PI R. Gilli, this is the largest Chandra program ever granted to any Italian institution). The main objectives of these observations were: i) obtaining the highest quality X-ray spectrum of a z > 6 QSO ever to study its physical properties; ii) verify the existence of satellite AGN in the candidate galaxy overdensity we previously measured around it (Balmaverde et al. 2017). We note that the Chandra survey in the J1030 field is actually the 4th deepest X-ray survey to date after the well- known 7Ms CDFS, 2Ms CDFN and 800ks AEGIS-X field. 3) The census of high-redshift quasars is still highly uncertain, due to the presence of high obscuration in a large fraction of sources. We present a novel approach to obtain a census of high-z SMBH unaffected by absorption, based on blazars. The particular orientation of blazars makes obscuration effects less relevant. Our objective is to obtain an unbiased space density of the entire population of radio-loud AGN directly from the observed number of blazars using the beaming formalism (Ghisellini et al. 2014). We are thus building up the largest sample of high-z blazar using a well- defined, flux-limited radio survey (CLASS, Myers et al. 2003).

2. Cosmology with quasars

In the past four years we obtained several fundamental results on the validation of the X-ray to UV relation in quasars and on its cosmological application:

First, we performed a complete analysis of the sample of $z \sim 3$ quasars with dedicated XMM-Newton observations (Nardini et al. 2019). The 30 quasars observed within our AO16 program were selected in the 3.0–3.3 redshift range, among the most luminous sources in the SDSS quasar catalogues, and with the requirement of "normal", blue rest-frame UV spectra, without any hint of dust absorption and/or other peculiar spectral property. The goal of this selection was to obtain reliable measurements of the fluxes at both 2500 Å and 2 keV (rest frame), chosen as the UV (disc) and X-ray (corona) emission proxies, respectively. Recently, in addition to the XMM-Newton and SDSS spectra, we obtained dedicated near-IR spectral observations at the LBT in the IJ band (for the whole sample) and in the K band (for 9 sources). The results of this multi-wavelength campaign are indeed remarkable, and partly surprising:

1) Out of the 30 observed objects, only 18 were selected for the inclusion in the Hubble diagram of quasars. This further selection is due to the requirement of an X-ray photon index $\Gamma > 1.7$, adopted for the whole Hubble diagram of quasars, and mainly aimed at excluding absorbed sources. Since none of the 30 sources had been observed in the X-rays before, we expected a few outliers, but the high fraction of sources with $\Gamma < 1.7$ has come as a surprise. The striking result is that all the "accepted" X-ray steep sources show a very small dispersion in the X-ray to UV relation, while all the excluded, X-ray flat ones have a much lower X-ray emission than predicted by the X-ray to UV relation.

2) In order to take full advantage of the results on the "accepted" sources, we built a "golden" sample in the same z=3.0–3.3 interval merging these 18 sources with the other quasars in the main sample. For these sources we performed a one-by-one spectral analysis in both the X-ray and UV bands, obtaining the most accurate flux estimates in the whole sample of 2,400 quasars. The results are shown in Fig. 1: the X-ray to UV relation for this golden sample is extremely tight, with a dispersion of just 0.1 dex, which can be entirely explained through variability and inclination effects. The lower panels of Fig. 1 compare the slope of the relation and the dispersion in the golden sample with those measured for the whole sample in other redshift intervals. We notice that the analysis of the relation in small redshift bins is cosmology-independent, because the distance differences are negligible within the same bin.

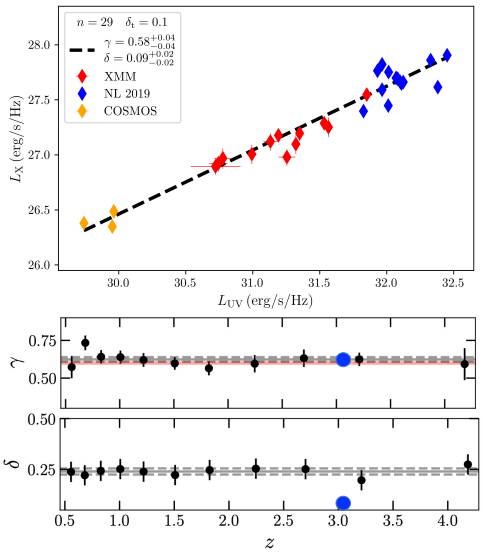

Fig. 1. Upper panel: X-ray to UV relation for a "golden" sample in the redshift range z=3.0–3.3. The very luminous quasars with dedicated XMM-Newton observations are the blue points. The blue points refer to the sources with pointed XMM observations. The dispersion of the relation is as small as 0.09 dex. Lower panels: Slope and dispersion of the relation in different redshift bins for the total sample. The blue point refers to the golden sample.

3) The distances estimated from the UV to X-ray relation for the z∼3 sample have been used to put these sources in the Hubble diagram, as shown in Fig. 2 (Risaliti & Lusso 2019). It is clear from the insets that these sources alone already constitute a $\sim 3\sigma$ deviation from the standard λCDM model.

4) The remaining z∼3 quasars with flat X-ray spectral slope have peculiar X-ray properties: their X-ray weakness, by a factor of at least 3–10 with respect to the UV to X-ray relation, is not consistent with photoelectric ab-

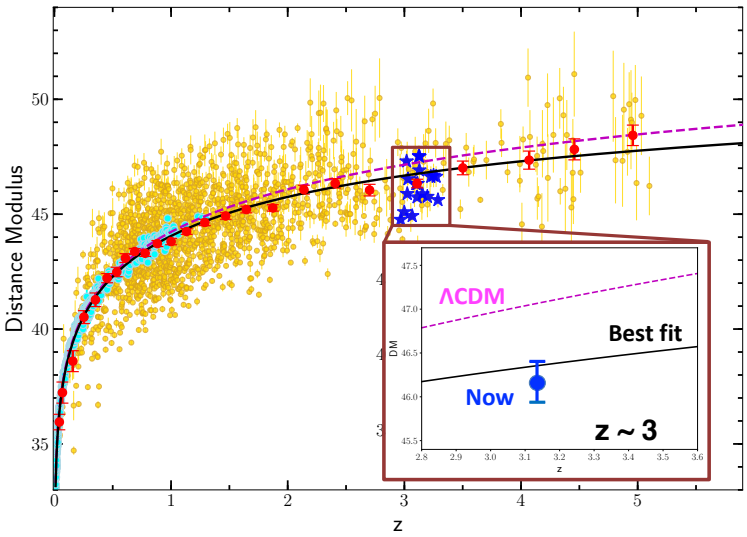

Fig. 2. Hubble diagram of supernovae and quasars. Cyan points: supernovae (Pantheon sample, Scolnic et al. 2018). Yellow points: quasars. Red points: average of quasars in small redshift bins, plotted to facilitate the comparison between the data and the models. The black and dashed-magenta lines are a cosmographic best-fit model and the standard ΛCDM model, respectively. The lower inset is a zoom of the z∼3 region, showing the average of the sources with XMM-Newton dedicated observations.

sorption, and is most likely intrinsic (Nar et al. 2019). The comparison of the spec emission lines of the two subsamples with 1.7 and Γ > 1.7 shows a significant dif ence between the average CIV emission l (Fig. 3). We interpret this results as the dence of a stronger outflowing wind in X- weak objects, which could be responsibl the broader emission lines, and of the de tion of seed UV photons illuminating the X- corona. In this scenario, the X-ray weak would be determined by the power of the cretion disk wind, possibly related to the f back at galactic scales.

A further line of analysis consisted in the definition of a new, larger sample for cosmological analysis. This work, published in Lusso et al. (2020), discussed all the criteria required to select a homogeneous sample of quasars for cosmological purposes and, on the other hand, the specific procedures adopted to compute the UV and X-ray fluxes and spectral slopes from the available photometry. We identified the quasars that can be used for a cosmological analysis, examined the key steps in fitting the distance modulus–redshift relation, and considered the possible systematics in the quasar Hubble-Lemaître diagram. In particular, we investigated in depth the residuals of the quasar Hubble diagram, in order to unveil any sys-

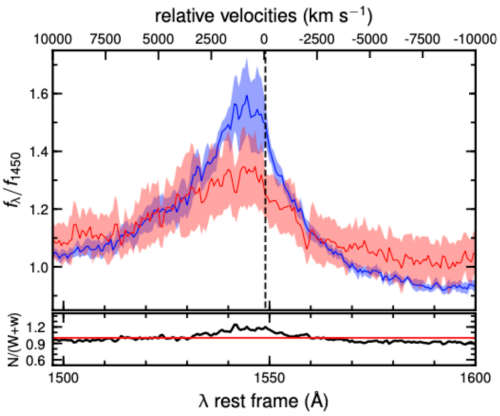

Fig. 3. Average C IV profile for the X-ray steep/bright sources (blue) and the X-ray flat/weak ones (red) in our z∼3 sample.

tematics unaccounted for in the selection of the sample. We explored whether our procedure to select blue quasars based on their SED shape, where dust absorption and host-galaxy contamination are minimised, introduces spurious trends in the Hubble diagram residuals as a function of redshift and for different intervals of the relevant parameters. Our main results are the following:
– We verified that the $L_X - L_{UV}$ relation (i.e. slope and dispersion) for the final best quasar sample does not evolve with redshift.
– We confirmed that, whilst the quasar Hubble diagram is well reproduced by a standard flat ΛCDM model (with Ω_M=0.3) up to z∼1.5, a statistically significant deviation emerges at higher redshifts, in agreement with our previous works (e.g. Risaliti & Lusso 2015; Lusso et al. 2019).
– We found that none of the adopted filters introduce strong systematics in the Hubble diagram residuals, and specifically where the quasars become the only contributors and the deviation from the standard ΛCDM is more significant (i.e. at z>1.5).

A third line of study consisted in the use of the new cosmological sample to test cosmological models through a cosmographic approach (Bargiacchi et al. 2021). Cosmography is a powerful tool for investigating the Universe kinematic and then for reconstructing the dynamics in a model- independent way. Our new measurements of quasars have populated the Hubble diagram up to high redshifts and the application of the traditional cosmographic approach has become less straightforward due to the large redshifts implied. We investigated this issue through an expansion of the luminosity distance–redshift relation in terms of orthogonal logarithmic polynomials. In particular, we pointed out the advantages of a new procedure called orthogonalization, and we showed that such an expansion provides a very good fit in the whole z=0-7.5 range to both real and mock data obtained assuming various cosmological models. Moreover, although the cosmographic series is tested well beyond its convergence radius, the parameters obtained expanding the luminosity distance–redshift relation for the ΛCDM model are broadly consistent with the results from a fit of mock data obtained with the same cosmological model. This provides a method for testing the reliability of a cosmographic function to study cosmological models at high redshifts, and it demonstrates that the logarithmic polynomial series can be used to test the consistency of the ΛCDM model with the current Hubble diagram of quasars and supernovae Ia. We confirmed a strong tension (at $> 4\sigma$) between the concordance cosmological model and the Hubble diagram at z>1.5. This tension is dominated by the contribution of quasars at z ¿ 2 and also starts to be present in the few supernovae Ia observed at z>1.

3. The deep field around SDSS J1030+0524

Among the >300 luminous QSOs discovered at $z > 5.7$, SDSS J1030+0524 at z=6.31 features by far the best multi-band coverage. This includes deep LBT, CFHT, HST, Spitzer, MUSE and ALMA data, a 0.5Ms Chandra/ACIS-I exposure, and 30hrs of JVLA observations. Together with many of the above mentioned datasets, our group first devised and then obtained the long Chandra and JVLA observations, which make J1030 one of the deepest extragalactic fields in the X-rays and in the radio band. As described below, the exquisite data quality allowed us to investigate with unprecedented detail the accretion physics and environment of a SMBH at cosmic dawn, investigate the feedback of an active SMBH at cosmic noon, and finally to perform legacy survey science, e.g. to search and find the as yet unknown population of obscured and moderately luminous AGN in the early Universe.

In Nanni et al. (2018) we presented the Chandra observations of the z=6.3 QSO, which is currently the deepest X-ray observation of a QSO at cosmic dawn. We found that the X-ray flux and spectrum changed significantly over past observations, when the QSO was brighter and softer. Such variability is completely unexpected for QSOs as luminous as SDSS J1030 (Paolillo et al. 2017), and it may be a hint of the fast, possibly chaotic accretion process that is needed to grow BHs to 10^{8-9} $M_\odot$ in less than one Gyr. Later on, we

were able to discover that the QSO is part of a spectroscopically confirmed large scale structure (LSS) of star forming galaxies that extends for several physical Mpc around it (Mignoli et al. 2020). This was long predicted by theory, as these early SMBHs are expected to form and grown within large dark matter halos in biased cosmic environments, but it was never seen unambiguously before. This discovery was in fact the subject of an ESO press release (#eso2016).

Together with that at z=6.3, we serendipitously discovered another remarkable structure in the field, namely a protocluster that is assembling around a z=1.7 FRII radio-galaxy (Gilli et al. 2019). The unique feature of this system is the presence of diffuse X-ray emission overlapping with one of the FRII radio lobes. Four protocluster members are aligned along the edge of the X-ray emission. All of them feature star formation rates (SFR) a factor 2-5 higher than what is observed in the other protocluster members and in main sequence galaxies at the same redshift. We interpreted the diffuse X-rays as protocluster gas that is shock-heated by the FRII jet, and the observed SFR enhancement as produced by the compression of the galaxies' ISM by the expanding shock. This may represent the first evidence of positive AGN feedback on multiple galaxies several hundreds of kpc from the black hole, and the result was featured in a Chandra press release (2019/11/26). Subsequently, by means of ALMA observations, we discovered additional protocluster members and a large reservoir of molecular gas in the FRII host. These data led us to infer that the protocluster will likely evolve into a $> 10^{14}$ $M_\odot$ cluster by z=0 and that the FRII is the progenitor of the brightest cluster galaxy (BCG) caught in its main assembly phase (D'Amato et al. 2020).

Finally, we exploited and are still exploiting the potential of the Chandra observations as a deep AGN legacy field. We published the catalog of X-ray sources and their multi-band counterparts in Nanni et al. (2020), investigated the spectral properties of a sub-sample of candidate obscured AGN (Peca et al. 2021), and finally released the spectroscopic and photometric redshifts of the Chandra sources (Marchesi et al. 2021). Further spectroscopic observations, especially of high-z AGN candidates, are ongoing.

Detailed information about the J1030 field, including the main results, data and catalog releases, and the full publication list, can be found at the project website: http://j1030-field.oas.inaf.it/

4. Parametrization of the Dark Energy EOS

To test if the accelerated expansion of the Universe is due to the cosmological constant or some more general dark energy model, it is necessary to take into account an evolving equation of state (EOS). In Demianski et al. (2020) we consider a flat cosmological model with a simple two parametric EOS proposed by Chevalier, Polarski and Linder (CPL Chevallier & Polarski 2001; Linder 2003)

$$w(z) = w_0 + w_1 \frac{z}{1+z}\,, \tag{1}$$

where w_0 and w_1 are constants to be determined by the fitting procedure. Therefore, in order to fit the cosmological parameters and investigate if the dark energy properties evolve with redshift we joined the quasar Hubble diagram previously described in Sec.2, with a gamma ray bursts Hubble diagram build up calibrating the so called Amati relation (Amati 2006) between the spectral peak energy and the isotropic-equivalent radiated energy (see Demianski et al. 2021). This relation has been studied extensively to confirm its validity, and address the selection and circularity problems affecting its usage in cosmological studies (e.g. Amati et al. 2019). We use a Bayesian approach based on the MCMC method, sampling the space of prameters by running three independent chains and using the Gelman-Rubin diagnostic approach to test their convergence. In Fig. 4 we plot the 2D $w_0 - w_1$ confidence regions. It turns out that ΛCDM model corresponding to $w_0 = -1$ and $w_1 = 0$, is disfavored at the 3σ confidence level.

A confirmation of these results comes from Muccino et al. (2021) who, using a sample of 174 gamma-ray bursts, show that while at

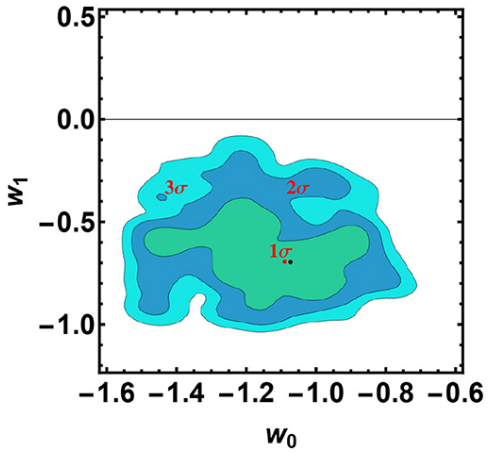

Fig. 4. Plot of the 2D $w_0 - w_1$ confidence regions. The red point corresponds to the best fit value and the mean respectively (from Demianski et al. 2020).

$z < 1.2$ $w(z)$ agrees within 1σ with the standard value $w = -1$, the situation is the opposite at larger z, where gamma-ray bursts better fix $w(z)$ that seems to deviate from $w = -1$ at 2σ and 4σ , depending on the redshift bins.

Further constraints coming from Gravitational Wave measurements are currently being explored, although to this date the highest redshift source is at $z \sim 0.49$ and thus not yet competitive with the Quasar and GRB samples. However Abbott et al. (2021) have shown to be able to constrain the Hubble parameter H_0 through the combination of binary black hole detections with galaxy catalogs obtaining $H_0 = 69^{+16}_{-8}$ km/s/Mpc establishing the path to cosmology using gravitational-wave observations.

5. Characterization of AGN variability

One of the uncertainties affecting the Hubble diagram of quasars is due to the intrinsic AGN variability. For such reason we investigated the timing properties of several samples of AGNs both in optical and X-rays with the aim of characterizing their behaviour and assessing its relation with cosmological parameters on one side and with the evolution of the host galaxies on the other. We expanded the work started in Chiaraluce et al. (2018) investigating the relation between X-rays and optical/UV luminosity using the combination of the *XMM-Newton Serendipitous Source Catalog* and the *XMM-OM Serendipitous Ultraviolet Source Survey*, that allowed to derive constraints on the uncertainty introduced in the Hubble Diagram. In Laurenti et al. (2020) we used the *Multi-Epoch XMM Serendipitous AGN Sample 2* (MEXSAS2) to extend the knowledge of the variability features of MEXSAS2 from the X-ray to the optical and search for correlations between variability and AGN physical quantities, i.e BH mass and bolometric luminosity, L_{Bol}. We found a significant decrease of variability amplitude with increasing bolometric, optical and X-ray luminosity. However when comparing optical to X-ray variability properties, we find that X-ray variability amplitude is approximately the same for those AGNs with larger or smaller variability amplitude in the optical. On the contrary, AGNs with steeper Structure Functions (SF) in the optical do present steeper SF in the X-ray, and vice versa. In Thomas et al. (2021) we extended these studies to high-z AGNs ($z \sim 4$) showing that these sources follow the usual trend of decreasing variability amplitude with increasing luminosity, and there is no evidence for X-ray variability increasing toward higher redshifts. In fact in our latest work in preparation (Paolillo et al. 2022) we are presenting evidence of a universal PSD model for both nearby and distant AGNs, over a wide range of luminosities and BH masses.

We further explored the variability detection efficiency in AGN samples, through the use of both classical and Machine Learning (ML) approaches. In De Cicco et al. (2019) we demonstrate to be able to select of high-purity (> 86%) samples based on variability alone, while the completeness w.r.t X-ray selected samples arrives to 59% and is mainly biased against obscured AGNs. Further improvements in the detection and classification approach were explored in Liu et al. (2020) and De Cicco et al. (2021), showing that ML methosd allow us to increase the completeness of our samples up to ∼ 70%.

The impact of variability studies extend beyond the characterization of the physical properties of the AGN themselves, providing constraints also on the coevolution between supermassive BHs and their host galaxies. We studied these issues assembling large sets of galaxies from both archival X-ray and optical data (Torbaniuk et al. 2021), as well as through dedicated large XMM campaigms (XMM-SERVS survey: Chen et al. 2018; Ni et al. 2021). Most notably in Georgakakis et al. (2021) we showed how ensemble variability measurements can strongly constrain both the BH vs stellar galaxy mass scaling relations, and the AGN PSD model (Fig. 5).

6. The census and evolution of high-z radio-loud AGN

Radio-loud AGN, i.e. accreting SMBH able to eject powerful relativistic jets, are a key ingredient to better understand the evolution of SMBH. If jets are produced in highly spinning black holes, SMBH hosted by RL AGN are expected to evolve differently from the rest of the population since the radiation efficiency should be higher (e.g. Thorne (1974)). For this reason, we want to study the evolutionary history of SMBH hosted by RL AGN up to high redshift (z∼6) and compare it with the total population of accreting SMBH. Nuclear obscuration is the most critical limitation to obtain a complete census of both RL and radio-quiet AGN. A powerful method to by pass this limit is to focus only on those RL AGN whose jet is pointed at small angles with respect to the our line-of-sight. Due to relativistic effects (beaming) the emission from these sources (called *blazars*) is strongly boosted and free from obscuration and can be observed up to very high redshift. From the number of observed blazars is then possible to infer, through geometrical arguments, the number of RL AGN pointing to all directions, including highly obscured ones (e.g. Ghisellini et al. 2014)

With this purpose, we have carried out a systematic search for high-z blazars by exploiting all the existing wide angle/all-sky radio (CLASS, NVSS, SUMSS, RACS), optical (PS1, DES) and infrared (WISE) surveys and using efficient photometric pre-selection techniques. All the photometric candidates have then been spectroscopically followed up using LBT and VLT to confirm the redshift. Finally, we have systematically observed the confirmed high-z AGN in the X-rays with Swift-XRT and, for the most distant ones, also with Chandra, to establish the blazar nature of the sources (Ighina et al. 2019; Ighina et al. 2021A, Ighina et al. 2021B; Moretti et al. 2021). In this way, we built the largest blazar sample ever selected containing ∼25 sources (Caccianiga et al. 2019; Belladitta et al. 2020; Ighina et al. 2021C) from z=4 up to z=6.1, the highest redshift discoverd so far in a blazar. Finally, we used the collected optical spectra to estimate the SMBH masses of all the discovered high-z blazars and for a consistently selected sample of lower redshift blazars, in order to trace, for the first time, the co-moving space density of the most massive SMBH ($> 10^9$ M_{sun}) hosted by all RL AGN from z∼1.5 up to z∼6 (Fig. 6, Diana et al. 2022; Belladitta et al. 2022). We found that the space density has a peak at z_{peak} ∼3.3, which is significantly larger than the value observed in the total AGN population with similar optical/UV luminosities (z_{peak} ∼2.2) thus confirming that SMBH in jetted AGN follow a different evolutionary path compared to the rest of the population. Interestingly, we observed a significant discrepancy compared to the space density evolution of blazars derived from the X-rays that hinted at even higher values of z_{peak} (>4, Ajello et al. 2009). A potential explaination for this discrepancy is that, at high redshifts, the X-ray luminosities are significantly boosted by the Inverse Compton interaction of the relativistic electrons of the jet with the photons of the Cosmic Microwave Background (Ighina et al. 2021A). A direct confirmation that this process is important at high z is the discovery of an extended X-ray jet in our Chandra observation of the blazar at z=6.1 (Ighina et al. 2021a) along the same direction of the extended radio jet that we discovered using high resolution imaging (Spingola et al. 2020). In addition, these Chandra obsevations have revealed a remarkable variability of the nucleus, possibly due to bulk Comptonization (Moretti

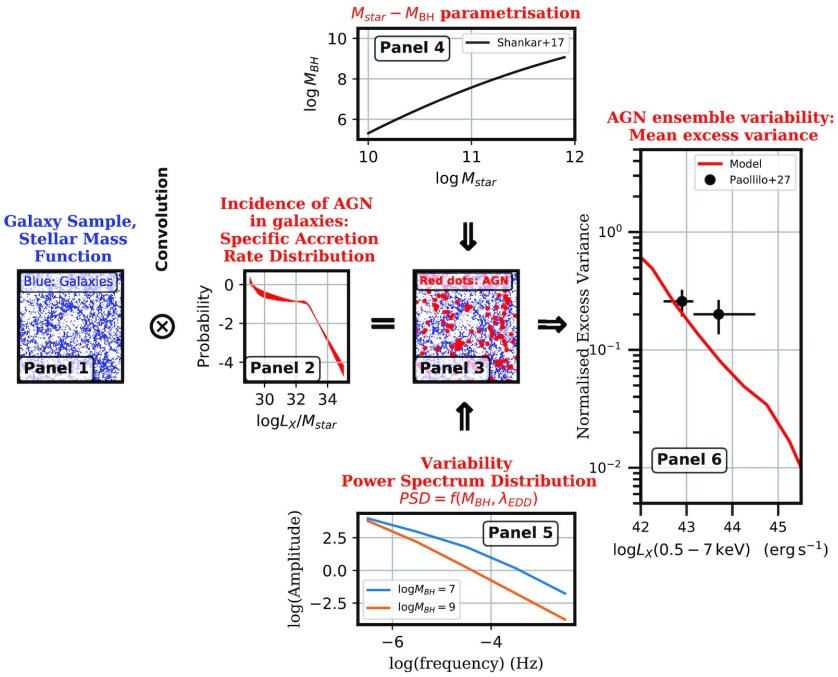

Fig. 5. Flowchart of the empirical AGN variability model from Georgakakis et al. (2021). The blue dots in panel 1 represent galaxies distributed in a cosmological volume. Combining this sample with the information on the black hole mass-stellar mass relation, the AGN incidence in galaxies, and their variability properties, it is possible to derive the average excess variance of the population binned in luminosity and redshift intervals (the solid line in panel 6). We refer to the original paper for a full description of the Figure.

et al. 2021). Although predicted by the emission models, it is the first time this process is actually observed through variability.

Acknowledgements. We acknowledge financial contribution from the agreement ASI-INAF n.2017-14-H.O.

References

Abbott, B. P., Abbott, R., Abbott, T. D., et al. 2021, ApJ, 909, 218
Ajello, M., Costamante, L., Sambruna, R. M., et al. 2009, ApJ, 699, 603
Amati, L. 2006, MNRAS, 372, 233
Amati, L., D'Agostino, R., Luongo, O., Muccino, M., & Tantalo, M. 2019, MNRAS, 486, L46
Balmaverde, B., Gilli, R., Mignoli, M., et al. 2017, A&A, 606, A23
Bargiacchi, G., Risaliti, G., Benetti, M., et al. 2021, A&A, 649, A65
Belladitta, S., Caccianiga, A., Diana, A., et al. 2022, arXiv e-prints, arXiv:2201.08863
Belladitta, S., Moretti, A., Caccianiga, A., et al. 2020, A&A, 635, L7
Caccianiga, A., Moretti, A., Belladitta, S., et al. 2019, MNRAS, 484, 204
Chen, C. T. J., Brandt, W. N., Luo, B., et al. 2018, MNRAS, 478, 2132
Chevallier, M. & Polarski, D. 2001, International Journal of Modern Physics D, 10, 213
Chiaraluce, E., Vagnetti, F., Tombesi, F., & Paolillo, M. 2018, A&A, 619, A95
D'Amato, Q., Gilli, R., Prandoni, I., et al. 2020, A&A, 641, L6
De Cicco, D., Bauer, F. E., Paolillo, M., et al. 2021, A&A, 645, A103
De Cicco, D., Paolillo, M., Falocco, S., et al. 2019, A&A, 627, A33

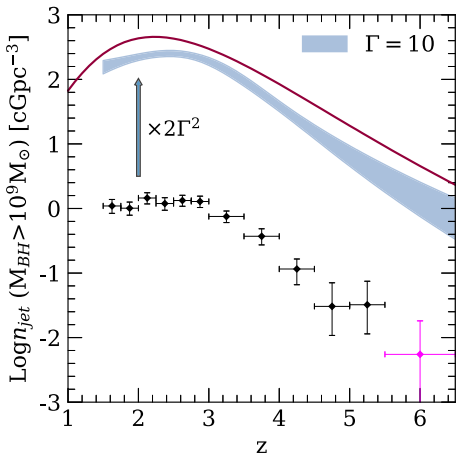

Fig. 6. Evolution of the space density of the most massive SMBH hosted in RL QSO (blue shaded area) derived in (Diana et al. 2022) using a radio flux limited sample of blazars from z∼1 to z=6 (black points). For comparison the red line reports the space density of the most massive SMBH hosted by the entire QSO population (red line). The comparison suggests a small but statistically significant difference in the peaks of the two curves with SMBH hosted by RL QSO reaching the maximum value earlier (z∼2.6-3) compared to the entire population (mostly composed by RQ QSO).

Demianski, M., Lusso, E., Paolillo, M., Piedipalumbo, E., & Risaliti, G. 2020, Frontiers in Astronomy and Space Sciences, 7, 69

Demianski, M., Piedipalumbo, E., Sawant, D., & Amati, L. 2021, MNRAS, 506, 903

Diana, A., Caccianiga, A., Ighina, L., et al. 2022, MNRAS, 511, 5436

Georgakakis, A., Papadakis, I., & Paolillo, M. 2021, MNRAS, 508, 3463

Ghisellini, G., Sbarrato, T., Tagliaferri, G., et al. 2014, MNRAS, 440, L111

Gilli, R., Mignoli, M., Peca, A., et al. 2019, A&A, 632, A26

Ighina, L., Belladitta, S., Caccianiga, A., et al. 2021a, A&A, 647, L11

Ighina, L., Caccianiga, A., Moretti, A., et al. 2019, MNRAS, 489, 2732

Ighina, L., Caccianiga, A., Moretti, A., et al. 2021b, MNRAS, 505, 4120

Ighina, L., Moretti, A., Tavecchio, F., et al. 2021c, arXiv e-prints, arXiv:2111.08632

Laurenti, M., Vagnetti, F., Middei, R., & Paolillo, M. 2020, MNRAS, 499, 6053

Linder, E. V. 2003, Phys. Rev. Lett., 90, 091301

Liu, D., Deng, W., Fan, Z., et al. 2020, MNRAS, 493, 3825

Lusso, E., Piedipalumbo, E., Risaliti, G., et al. 2019, A&A, 628, L4

Lusso, E. & Risaliti, G. 2016, ApJ, 819, 154

Lusso, E., Risaliti, G., Nardini, E., et al. 2020, A&A, 642, A150

Marchesi, S., Mignoli, M., Gilli, R., et al. 2021, A&A, 656, A117

Mignoli, M., Gilli, R., Decarli, R., et al. 2020, A&A, 642, L1

Moretti, A., Ghisellini, G., Caccianiga, A., et al. 2021, ApJ, 920, 15

Muccino, M., Izzo, L., Luongo, O., et al. 2021, ApJ, 908, 181

Myers, S. T., Jackson, N. J., Browne, I. W. A., et al. 2003, MNRAS, 341, 1

Nanni, R., Gilli, R., Vignali, C., et al. 2018, A&A, 614, A121

Nanni, R., Gilli, R., Vignali, C., et al. 2020, A&A, 637, A52

Nardini, E., Lusso, E., Risaliti, G., et al. 2019, A&A, 632, A109

Ni, Q., Brandt, W. N., Chen, C.-T., et al. 2021, ApJS, 256, 21

Paolillo, M., Papadakis, I., Brandt, W. N., et al. 2017, MNRAS, 471, 4398

Peca, A., Vignali, C., Gilli, R., et al. 2021, ApJ, 906, 90

Risaliti, G. & Lusso, E. 2015, ApJ, 815, 33

Risaliti, G. & Lusso, E. 2019, Nature Astronomy

Scolnic, D. M., Jones, D. O., Rest, A., et al. 2018, ApJ, 859, 101

Spingola, C., Dallacasa, D., Belladitta, S., et al. 2020, A&A, 643, L12

Thomas, M. O., Shemmer, O., Brandt, W. N., et al. 2021, ApJ, 923, 111

Thorne, K. S. 1974, ApJ, 191, 507

Torbaniuk, O., Paolillo, M., Carrera, F., et al. 2021, MNRAS, 506, 2619

Wu, X.-B., Wang, F., Fan, X., et al. 2015, Nature, 518, 512